 ICCES, vol.14, no.2, pp.43-49

On essential work of fracture method: theoretical consideration and numerical simulation

X.-H. Chen[1], Y.-W. Mai[2]

Summary

A general elastoplastic fracture mechanics theory is proposed for applying the Essential-Work-of-Fracture (EWF) Method to quasi-static and impact toughness characterization. Advanced finite element modeling is developed to simulate the EWF Method using the crack-tip opening angle criterion (CTOA) and the constitutive relation of the material under consideration. For Poly(ethylene-terephlate) (PET) films, the load-displacement curves are calculated for the whole crack propagation process of deeply double-edge notched tensile specimens (DENT) with different ligament lengths so as to determine the total work, the essential work and the non-essential work of fracture. The effects of specimen gauge length and ligament length on crack growth stability are also discussed in combination with experimental results.

Keywords: Essential Work of Fracture Method; Finite Element Modeling; Crack Propagation; Elastoplastic Fracture Mechanics.

Introduction

The Essential-Work-of-Fracture method, developed by Cotterell, Mai and coworkers (Cotterell & Reddel, 1977; Mai & Cotterell, 1980, 1986; Mai *et al.*, 2000) based on the original ideas of Broberg (1971, 1975), has been widely used for fracture characterization of thin metal sheets, polymeric films, paper sheets, toughened plastics and blends. The advantage of this technique by separating the total work into the essential work consumed in the inner fracture process zone and the non-essential work dissipated in the outer region lies in its experimental simplicity and the ease of test data analysis.

Chan and Williams (1994), Karger-Kocsis and Czigany (1996), Hashemi (1997) and Ching *et al.* (2000) studied the effects of gauge length and loading rate on the essential fracture work measurement of several ductile polymers. Specifically, Ching *et al.* (2000) observed that by increasing the gauge length of the Poly(ethylene-terephlate) (PET) samples crack growth became unstable for some ligament lengths

[1]University of Sydney, Sydney, NSW 2006, Australia. Current address: Sikorsky Aircraft Corporation, Stratford, CT, U.S.A.

[2]University of Sydney, Sydney, NSW 2006, Australia; and Hong Kong Polytechnic University, Hung Hom, Kowloon, Hong Kong.

leading to the occurrence of ductile-brittle fracture transition. In contrast, Knockaert *et al*. (1996) studied the fracture behavior of deeply double-edge notched tension steel plates, both experimentally and numerically. However, since the load-displacement curves were calculated only to the maximum load, the total work of fracture, the essential and non-essential works of fracture could not be obtained. Chen *et al*. (1999) overcame this difficulty and provided a full numerical simulation of the essential fracture work method for high-density polyethylene thin sheets (Mai and Powell, 1991). The objectives of this paper are to provide further theoretical consideration and numerical simulation of the Essential-Work-of-Fracture method and compare analytical predictions with experimental results obtained by Ching *et al*. (2000).

Theoretical consideration

As an extension of the previous studies by Nguyen *et al*. (2005) and Simha *et al*. (2008), the Helmholtz free energy is taken to be a function of the elastic Lagrange strain tensor, $\mathrm{E}^e = (F^{eT}F^e - I)/2$, and the absolute temperature, T, with the isotropic hardening parameter, p, and the back strain tensor, α, as internal variables:

$$\hat{h} = \hat{h}(\mathrm{E}^e, T, p, \alpha) \tag{1}$$

where multiplicative decomposition of the deformation gradient into elastic and plastic parts is adopted, that is, $F = F^e F^p$.

Consider a body $\tilde{B}$ that contains an extending crack. The contour $\tilde{\Gamma}$ translates with the crack tip moving at a speed $\mathbf{c}$. Based on the fundamental principles of thermodynamics, the energy flux integral can be expressed as:

$$\begin{aligned} F(\tilde{\Gamma}) \equiv & \int_{\tilde{\Gamma}} [n\cdot\sigma\cdot v + (\tilde{\rho}\hat{h} + \tilde{\rho}\hat{k})n\cdot c]d\tilde{\Gamma} \\ &= \int_{\partial\tilde{B}} n\cdot\sigma\cdot v d\tilde{S} - \int_{\tilde{B}-\tilde{V}_{\tilde{\Gamma}}} \frac{\tilde{\partial}}{\tilde{\partial} t}(\tilde{\rho}\hat{h} + \tilde{\rho}\hat{k})d\tilde{V} + \int_{\tilde{B}-\tilde{V}_{\tilde{\Gamma}}} \tilde{\rho}\hat{f}\cdot v d\tilde{V} \\ &\quad - \int_{\tilde{B}-\tilde{V}_{\tilde{\Gamma}}} (\tau_{ij}D^p_{ij} + \hat{x}_{ij}\dot{\alpha}_{ij} + \hat{y}\dot{p})d\tilde{V} - \int_{\tilde{B}-\tilde{V}_{\tilde{\Gamma}}} \tilde{\rho}\hat{s}\dot{T}d\tilde{V} \end{aligned} \tag{2}$$

where $v = \dot{u}$ is velocity vector; σ Cauchy stress tensor; $\tau = J\sigma$ Kirchhoff stress tensor; $D^p = (L^p + L^{pT})/2$; $L^p = F^e\dot{F}^pF^{p-1}F^{e-1}$; $J = \tilde{\rho}/\rho$ in which ρ is the mass density in current configuration; $\tilde{\rho}$ mass density in reference configuration; $\hat{f}$ mechanical body force per unit mass; $\hat{k}$ kinetic energy per unit mass; $\hat{s}$ entropy per unit mass; $\hat{y}$ and $\hat{x}_{ij}$ are thermodynamic forces conjugate to the isotropic hardening parameter p and the back strain tensor α, respectively.

The dynamic contour integral is related to the energy flux integral by:

$$\tilde{J}_{\tilde{\Gamma}} = \frac{F(\tilde{\Gamma})}{Bc} = \frac{1}{Bc}\int_{\tilde{\Gamma}}[n\cdot\sigma\cdot v+(\tilde{\rho}\hat{h}+\tilde{\rho}\hat{k})n\cdot c]d\tilde{\Gamma} \tag{3}$$

where $c = |c|$, and B is the thickness along the crack front.

Following Freund (1998), the dynamic energy release rate is defined as the rate of energy flow out of the body and into the fracture process zone per unit crack advance:

$$\tilde{J}_0 = \lim_{\tilde{\Gamma}\to\tilde{\Gamma}_0}\left\{\frac{1}{Bc}\int_{\tilde{\Gamma}}[n\cdot\sigma\cdot v+(\tilde{\rho}\hat{h}+\tilde{\rho}\hat{k})n\cdot c]d\tilde{\Gamma}\right\} \tag{4}$$

The relationship between the global and local dynamic contour integrals is obtained from:

$$\begin{aligned}\tilde{J}_g &- \frac{1}{Bc}\int_{\tilde{V}_g}\left[\frac{\tilde{\partial}}{\tilde{\partial}t}(\tilde{\rho}\hat{h}+\tilde{\rho}\hat{k})-\tilde{\rho}\hat{f}\cdot v+(\tau_{ij}D^p_{ij}+\hat{x}_{ij}\dot{\alpha}_{ij}+\hat{y}\dot{p})+\tilde{\rho}\hat{s}\dot{T}\right]d\tilde{V}\\ &= \tilde{J}_l - \frac{1}{Bc}\int_{\tilde{V}_l}\left[\frac{\tilde{\partial}}{\tilde{\partial}t}(\tilde{\rho}\hat{h}+\tilde{\rho}\hat{k})-\tilde{\rho}\hat{f}\cdot v+(\tau_{ij}D^p_{ij}+\hat{x}_{ij}\dot{\alpha}_{ij}+\hat{y}\dot{p})+\tilde{\rho}\hat{s}\dot{T}\right]d\tilde{V}\\ &= \tilde{J}_0\end{aligned} \tag{5}$$

where $\tilde{V}_g$ and $\tilde{V}_l$ are the volumes bounded by the closed surfaces $\tilde{\Gamma}_g$ and $\tilde{\Gamma}_l$ including the crack faces.

For steady-state crack propagation along the $\tilde{e}_1$–direction, the dynamic contour integral expression takes the special form:

$$\tilde{J}_{\tilde{\Gamma}} = \frac{1}{B}\int_{\tilde{\Gamma}} n\cdot[-\sigma\cdot u\tilde{\nabla}+(\tilde{\rho}\hat{h}+\tilde{\rho}\hat{k})I]d\tilde{\Gamma}\cdot\tilde{e}_1 \tag{6}$$

Hence, the dynamic energy release rate serves as the thermodynamic driving force for crack propagation in elastoplastic materials, which can be taken as the time-continuous counterpart to the discrete path-domain independent integral developed by Simo and Honein (1990) as well as the dynamic counterpart to the quasi-static global material (configuration) force given by Nguyen *et al.* (2005) and Simha *et al.* (2008).

The conditions for stable crack propagation can be expressed as:

$$\tilde{J}_0 = J_c \tag{7}$$

$$\frac{d\tilde{J}_g}{da} - \frac{dJ_R}{da} \leq 0 \tag{8}$$

Unstable crack growth occurs when

$$\frac{d\tilde{J}_g}{da} - \frac{dJ_R}{da} > 0 \tag{9}$$

The global energy balance equation can be written by:

$$\frac{dW}{dt} = \frac{dH}{dt} + \frac{dK}{dt} + \int_{\tilde{V}} (\tau_{ij} D^p_{ij} + \hat{x}_{ij}\dot{\alpha}_{ij} + \hat{y}\dot{p}) d\tilde{V} + \int_{\tilde{V}} \tilde{\rho}\hat{s}\dot{T} d\tilde{V} + J_c\dot{A} \tag{10}$$

where W is external work, H is Helmholtz free energy, and K is kinetic energy.

As the time frame is taken from the start of loading, t_0, till final fracture, t_f, the total work of fracture, W_f, can be partitioned into the essential work of fracture, W_e, and the non-essential work of fracture, W_{ne}, that is,

$$W_f = W_e + W_{ne} \tag{11}$$

$$W_e = \int_{t_0}^{t_f} w_e \dot{A} dt = \int_{t_0}^{t_f} J_c \dot{A} dt \tag{12}$$

$$W_{ne} = \Delta H + \Delta K + \int_{t_0}^{t_f} dt \int_{\tilde{V}} (\tau_{ij} D^p_{ij} + \hat{x}_{ij}\dot{\alpha}_{ij} + \hat{y}\dot{p}) d\tilde{V} + + \int_{t_0}^{t_f} dt \int_{\tilde{V}} \tilde{\rho}\hat{s}\dot{T} d\tilde{V} \tag{13}$$

Hence, the specific essential work of fracture is equivalent to the critical value of the dynamic contour integral, whereas the non-essential work of fracture is a sum of Helmholtz free energy change, kinetic energy change, plastic dissipation, and thermal dissipation. The EWF method can be conveniently used for the characterization of plane-stress fracture toughness for ductile metals, paper and plastic sheets with deeply-cracked specimens, where the height of the outer plastic region is proportional to the ligament length l. Thus, the specific total fracture work w_f(=W_f/Bl) is given by:

$$w_f = w_e + \beta w_p l \tag{14}$$

where w_e and βw_p are the specific essential and specific non-essential work of fracture, respectively. Assuming that w_e is a material property and that w_p and β are independent of l in all tested samples, there should exist a linear relationship when w_f is plotted against l.

Numerical simulation

The elastoplastic crack growth analysis was performed using the ABAQUS commercial software package with the "DEBOND" and "FRACTURE CRITERION" options for DENT samples, as shown in Fig. 1. Based on experimental observation (Ching *et al.*, 2000), we set the crack opening displacement to 1.07 mm at a distance of 1.35 mm behind the current crack tip, which corresponds to a constant critical crack-tip opening angle (CTOA) of 23^o. All the specimens have a thickness (B) of 0.5 mm and a width (W) of 50 mm. The ligament length (l) varies from 5 mm to 24.8 mm.

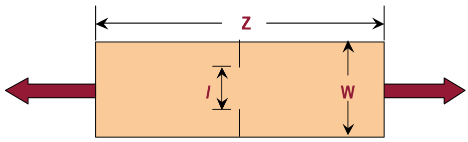

Figure 1: DENT Specimen

The numerical load-displacement curves ($P \sim \Delta$) are obtained for the DENT samples with selected ligament lengths at gauge lengths (Z) of 100, 150, 200 mm (Fig. 2a). When crack growth is stable throughout the fracture process, all these curves have similar shapes and the steep stress-drops after the maximum load are well simulated. Unstable crack growth leading to the ductile-brittle fracture transition is reflected by the precipitous load-drops for l= 24.8 mm at a gauge length of 150 mm. It is noted that simulation was conducted only up to the maximum load for ligament length of 24.8 mm due to difficulty of obtaining numerical convergence. The numerical load-displacement curves compare favorably with the experimental load-displacement curves (Ching *et al*., 2000). The areas under these curves can be calculated by integration to plot the specific total fracture work (w_f) against ligament length (l) in Fig.2b. The two vertical dashed lines denote the valid range of ligament length, $5t$ $(= 2.5 \text{ mm}) \leq l \leq W/3$ $(= 16.6 \text{ mm})$, within which the data points were used for the linear regression analysis.

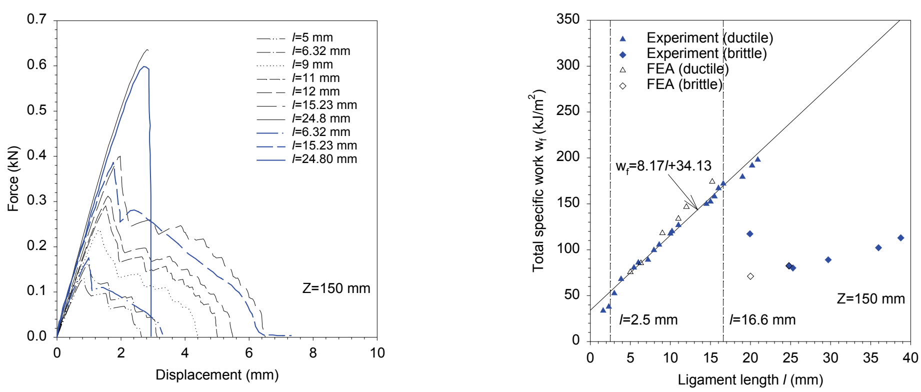

Figure 2: (a) Load-displacement curves and (b) specific total fracture work against ligament length for DENT samples at gauge length Z=150 mm

The numerical specific essential work of fracture (w_e) and non-essential work of fracture (βw_p), are listed in Table 1 for the three gauge lengths of 100, 150 and

200 mm in comparison with the experimental data. It is noted that the calculated total specific works of fracture are somewhat larger than the experimental values at long ligament lengths. This subsequently leads to the predictions of a lower specific essential fracture work but a higher specific non-essential fracture work when compared to the corresponding regression values based on the experimental data.

Table 1: Comparisons of numerical and experimental w_e (kJ/m^2) and βw_p (MJ/m^3)

Gauge length	w_e		βw_p	
	Exp.	Num.	Exp.	Num.
Z=100 mm	29.84	27.38	8.11	9.64
Z=150 mm	34.13	26.20	8.17	9.85
Z=200 mm	33.98	24.48	7.53	10.28

The contour plots in the central ligament region around the crack tip in DENT specimen with ligament length of 15.23 mm for Von Mises stress just prior to crack initiation and equivalent plastic strain at final failure are shown in Fig.3a and 3b. It is clear that prior to crack initiation the ligaments in these samples have fully yielded. The large plastic deformations of the fracture specimens obtained by numerical simulation are consistent with the experimental observations.

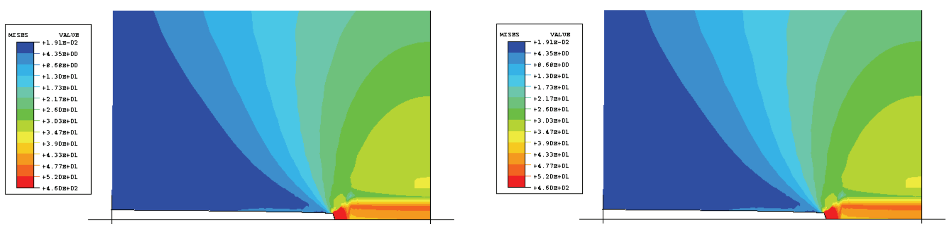

Figure 3: (a) Von Mises stress just prior to crack initiation and (b) equivalent plastic strain at final failure in the central ligament region around the crack tip in DENT specimen.

Concluding Remarks

The proposed general elastoplastic fracture mechanics theory provides the guidelines to extend the Essential-Work-of-Fracture method to quasi-static and impact fracture characterization of ductile materials under isothermal and non-isothermal conditions. Finite element results of load-deflection curves for a PET using the DENT specimen geometry with different gauge lengths and ligament lengths have been obtained based on the CTOA criterion. These simulated curves fit well with available experimental data. Linear dependence of the specific total fracture work

(w_f) on ligament length (l) is found for all three gauge lengths from the numerical simulation of stable crack growth. The ductile-brittle fracture transition may be affected by varying specimen gauge length and ligament length, which needs further investigation for future work.

References

1. **Broberg, K.B.** (1971): *J. Mech. Phys. Solids*, vol. 19, pp. 407-418.
2. **Broberg, K.B.** (1975): *J. Mech. Phys. Solids*, vol. 23, pp. 215-237.
3. **Chan, W. Y. F.; Williams, J. G.** (1994): *Polymer*, vol. 35, pp. 1666-1672.
4. **Chen, X.-H; Mai, Y.-W.; Tong, P.; Zhang, L.-C.** (1999): In: *Fracture of Polymers, Composites and Adhesives*, ESIS 27, edited by J.G. Williams and A. Pavan, Elsevier, Amsterdam, 2000.
5. **Ching, E. C.-Y.; Li, R. K.-Y.; Mai, Y.-W.** (2000): *Polymer Engineering and Science*, vol. 40, pp. 310-319.
6. **Cotterell, B.; Reddel, J. K.** (1977): *Int. J. Fract.*, vol. 13, pp. 267-277.
7. **Freund, L.B.** (1998): *Dynamic Fracture Mechanics*, Cambridge University Press, Cambridge.
8. **Hashemi, S.** (1997): *Polymer Engineering and Science*, vol. 37, pp. 912-921.
9. **Karger-Kocsis, J.; Czigany, T.** (1996): *Polymer*, vol. 37, pp. 2433-2438.
10. **Knockaert, R.; Doghri, I.; Marchal, Y.; Pardoen, T.; Delannay, F.** (1996): *Int. J. Fract.*, vol. 81, pp. 383-399.
11. **Mai, Y.-W.; Cotterell, B.** (1980): *Journal of Material Science*, vol. 15, pp. 2296-2306.
12. **Mai, Y.-W.; Cotterell, B.** (1986): *Int. J. Fract.*, vol. 32, pp. 105-125.
13. **Mai, Y.-W.; Powell, P.** (1991): *Journal of Polymer Science, Part B: Polymer Physics*, vol. 29, pp.785-793.
14. **Mai, Y.-W.; Wong, S.C.; Chen**, **X.H.** (2000): in *Polymer Blends,* DR Paul and CB Bucknall, *eds*., Volume 2, Chapter 20, John Wiley & Sons, New York.
15. **Nguyena, T.D.; Govindjeeb, S.; Kleinc, P.A.; Gao, H.** (2005): *J. Mech. Phys. Solids*, vol. 53, pp. 91-121.
16. **Simha, N.K.; Fischer, F.D.; Shan, G.X.; Chen, C.R.; Kolednik, O.** (2008): *J. Mech. Phys. Solids*, vol. 56, pp. 2876-2895.
17. **Simo, J.C.; Honein, T.** (1990): *J. Appl. Mech.*, vol. 57, pp. 488-497.